SSRG International Journal of Electrical and Electronics Engineering
ISSN: 2348-8379/ https://doi.org/10.14445/23488379/IJEEE-V12I10P108

Volume 12 Issue 10, 94-109, October 2025

Original Article

Goal-Seeking and Obstacle Avoidance Behaviour Using ORB Feature Extraction Approach for Improved Localization of Landmine Detection Mobile Robot

C.N. Naga Priya, S. Denis Ashok*

[1,2]*Department of Design and Automation, School of Mechanical Engineering (SMEC), Vellore Institute of Technology, Vellore, Tamil Nadu, India.*

* *Corresponding Author : denisashok@vit.ac.in*

Received: 05 August 2025 Revised: 07 September 2025 Accepted: 07 October 2025 Published: 30 October 2025

Abstract - *Unexploded buried landmines continue to pose a severe threat to human safety and the environment, while conventional manual detection methods remain slow, hazardous, and resource-intensive. Autonomous mobile robots equipped with advanced sensing capabilities provide a safer and more efficient alternative; however, achieving robust mine localization in open outdoor environments remains difficult due to sparse features, irregular terrain, and natural obstacles that complicate navigation. This work introduces a novel approach that integrates thermal–visual perception with adaptive path planning to address these challenges. Binary occupancy grid maps are generated from thermal imagery to provide a reliable environmental representation under varying lighting conditions. An Artificial Neural Network (ANN) is employed for hotspot detection, while ORB-based feature extraction and feature matching enable accurate camera pose estimation for visual localization. The proposed system fuses thermal and visual data to detect potential landmine signatures and natural obstacles in real time. A Rapidly-Exploring Random Tree (RRT) path planning algorithm is incorporated to ensure safe navigation across uneven terrain while avoiding hazards such as rocks and stones. Real-time decision-making is facilitated by thermal imaging, which enhances the localization of potential mine concentrations. Simulation results demonstrate the effectiveness of this integrated framework in simultaneously identifying buried landmines and planning safe traversable paths. By combining ANN-based classification, ORB feature matching, and RRT-based planning, the system achieves consistent classification of hazardous hotspots while dynamically adapting navigation strategies. The proposed approach represents a significant advancement toward reliable, autonomous landmine detection and contributes to enhancing safety in mine-contaminated regions.*

Keywords - *ORB feature extraction, ANN classification, Multi-goal seeking RRT, Landmine detection, Mobile robot.*

1. Introduction

Landmines remain a persistent threat in many post-conflict regions, endangering both human lives and environmental stability. Manual demining techniques are still widely used, despite being labour-intensive, slow, costly, and extremely hazardous to personnel [1, 2]. To overcome these limitations, autonomous mobile robotic systems have emerged as a promising alternative, offering safer and more efficient detection capabilities through the integration of advanced sensing, mapping, and navigation technologies [3, 4]. While various sensing methods have shown potential for landmine detection, a universally reliable solution remains elusive, especially in open outdoor terrains. In such environments, visual texture is sparse, GPS signals can be unreliable, and natural obstacles such as vegetation and uneven ground complicate perception and autonomous navigation. Although there are advances in sensing and navigation, two critical research gaps persist. First, most existing works include thermal sensing, feature-based localization, classification, and motion planning as isolated modules, which limits overall system robustness in unpredictable, GPS-denied conditions. Second, there is limited research on integrated frameworks that combine perception and navigation to allow robots to simultaneously detect, classify, and safely traverse cluttered, unstructured terrains in real time.

2. Literature Review

Multiple sensing modalities have been extensively studied to address the challenges of landmine detection. Ground-Penetrating Radar (GPR) uses radio wave reflections to detect subsurface anomalies and has demonstrated high accuracy in controlled settings [5, 6]. However, its performance deteriorates in heterogeneous or cluttered soils, limiting robustness in realistic outdoor conditions. Thermal imaging has emerged as a complementary sensing method that senses the temperature contrasts between buried landmines

and surrounding soils, offering advantages under challenging conditions such as fog, mist, or nighttime when visual cues diminish [7, 8]. The passive nature of thermal sensors enables the detection of heat signatures generated by solar heating or thermal inertia difference, aiding in the identification of hazardous objects. Several studies have demonstrated that thermal cameras, when combined with advanced image processing, enhance detection reliability, especially in open terrains with sparse visual texture [9, 10].

Vision-based systems, which utilize deep learning and classical feature extraction techniques, have also gained traction for landmine detection. Deep Convolutional Neural Networks (CNNs) enhance object classification capabilities using both visible and infrared imagery, addressing the limitations of traditional handcrafted features [11, 12]. Among feature descriptors, Oriented FAST and Rotated BRIEF (ORB) has been widely adopted for its computational efficiency and robustness in low-texture environments compared to SIFT or SURF [13, 14]. ORB estimates the camera pose by matching keypoints across successive frames, enabling reliable visual localization necessary for autonomous navigation [9, 15]. Effective autonomous landmine detection requires robust sensing and classification, and reliable localization and motion planning in complex, unstructured environments. Advances in sampling-based motion planning algorithms, particularly Rapidly Exploring Random Tree (RRT) variants such as enhanced RRT and EB-RRT, have shown promise for traversing cluttered terrains [16-19]. However, most existing approaches treat perception and planning as separate modules without tight integration, resulting in limited adaptability during real-time operation.

Occupancy grid mapping, constructed from sensory inputs like thermal imagery, provides a spatial representation of obstacles and hotspots that can be leveraged for informed path planning and obstacle avoidance [20-22]. Integration of fuzzy logic into classification pipelines improves decision-making under uncertainty by interpreting thermal intensity variations, further enhancing detection specificity. Complementary research in multi-agent systems and sensor fusion techniques highlights the potential for scalable and robust demining architectures leveraging heterogeneous data sources [2, 23]. Despite significant advances, existing frameworks often lack a cohesive integration of thermal sensing, visual localization, intelligent classification, and adaptive motion planning in a manner that enables real-time, autonomous operation in GPS-denied and visually sparse outdoor environments. The dynamic and unpredictable nature of natural terrains demands an end-to-end solution that robustly fuses perception and navigation, adapting to changing conditions and obstacle configurations dynamically [24-26]. This research addresses these gaps by proposing a novel integrated framework that combines thermal imaging, ORB-based feature extraction, Artificial Neural Networks (ANN) for mine classification, and a multi-goal-seeking RRT-based navigation strategy. The framework constructs binary occupancy grid maps from thermal images to represent hotspots and obstacles, employs ORB features for robust camera localization without GPS dependency, and utilizes an ANN to classify landmines (buried and surface) as well as natural obstacles. Finally, an improved multi-goal-seeking RRT dynamically adapts robot navigation, ensuring safe traversal in cluttered outdoor terrains.

By unifying sensing, classification, localization, and planning into a single pipeline, this work enhances detection accuracy, strengthens autonomy in GPS-denied environments, and supports adaptive mission execution. The main contribution lies in bridging the gap between perception and planning for landmine detection robots, offering a step towards safer, more efficient, and intelligent autonomous demining operations.

3. Automated Mine Detection Approach

The proposed automated mine detection framework is developed for a mobile robot designed to operate in unstructured, GPS-denied outdoor environments where visual cues are limited. The system employs a thermal camera as the primary sensing unit, capturing heat signatures to distinguish buried and surface landmines from surrounding soil under adverse conditions such as fog, mist, or nighttime operations. The raw thermal input is enhanced through ORB-based feature extraction, which provides robust visual localization by tracking consistent feature points across consecutive image frames.

For classification, an ANN processes thermal imagery to accurately differentiate between buried landmines, surface landmines, and environmental obstacles such as rocks and vegetation. This perception module is coupled with a multi-goal seeking RRT planner, generating collision-free, adaptive paths toward multiple targets in real time. Unlike conventional RRT or RRT* algorithms, which either treat objectives independently or lack direct integration with perception data, the proposed planner biases its sampling toward unreached goals while incorporating obstacle information derived from the classification stage. This integration improves sampling efficiency, reduces redundant exploration, and ensures safe traversal in cluttered outdoor terrains. Figure 1 illustrates the schematic architecture, highlighting the seamless interaction between sensing, classification, and planning modules. Combining thermal sensing, ORB-based localization, ANN-based classification, and multi-goal RRT path planning into a single unified system, the proposed methodology addresses the challenges of mine detection accuracy, reliable localization, and adaptive navigation. This cohesive integration enables the robot to identify potential landmine hotspots and simultaneously plan safe paths across complex environments, marking a significant methodological advancement over fragmented approaches in the literature.

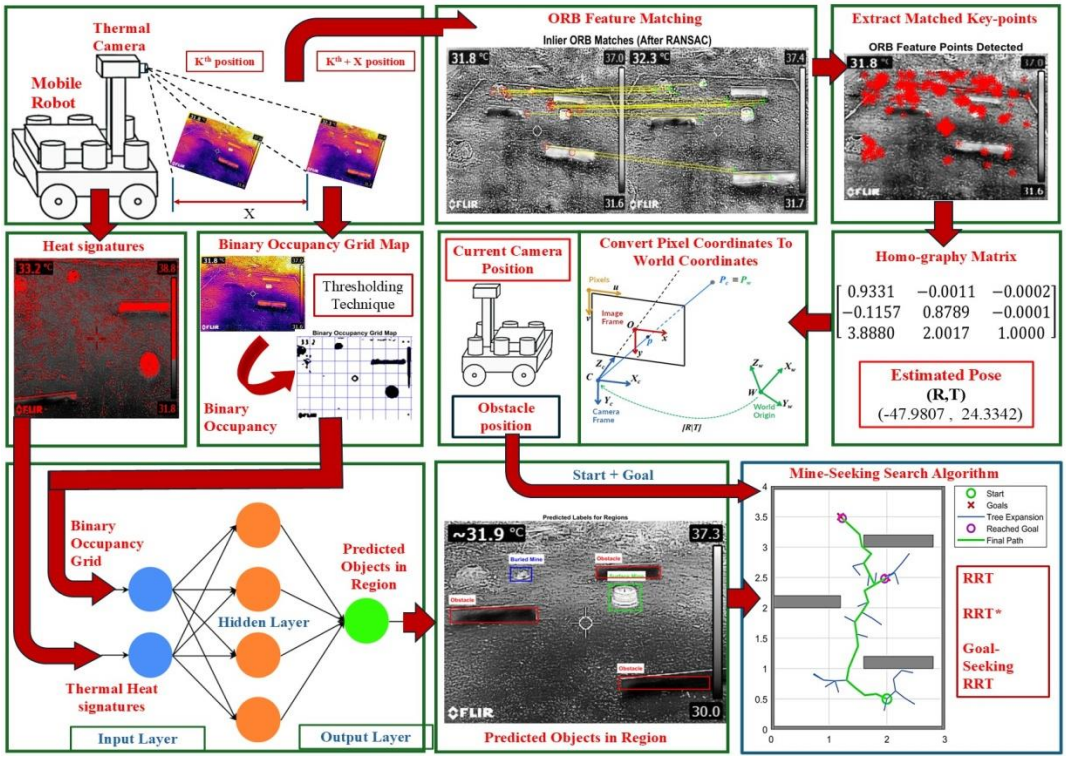

Fig. 1 Proposed ORB-based feature matching for a landmine detection mobile robot

3.1. ORB-Based Feature Extraction for the Localization of Buried Land Mines

The ORB-based feature extraction approach is followed for real-time automated detection of important visual features using thermal images and localization of buried land mines and mobile robots. By incorporating ORB feature mapping from consecutive images, the current position of the mobile robot can be estimated in the absence of a GPS signal or odometry data. ORB is a fast and powerful feature detection and description algorithm combining complementary techniques such as FAST as a keypoint detector and BRIEF as a feature descriptor. The proposed ORB-based Feature matching approach involves the following steps.

3.1.1. Image Pre-Processing

Thermal images are converted to a grayscale single-channel format representing temperature difference, which focuses on intensity, as the computational cost of grayscale images is simpler, which can speed up the analysis. Contrast enhancement & noise reduction methods like Gaussian filtering, contrast stretching, and histogram equalization are applied for a reliable feature detection method, depending on the visibility of temperature gradients and noise reduction; hence, this phase helps with both.

3.1.2 Keypoint Detection with ORB

ORB detects keypoints where there is a sharp shift in intensity by means of the FAST technique based on corner and edge detection. FAST is the corner detection method that uses the difference in pixel intensities to find keypoints in an image, while BRIEF generates a binary string for every key point based on simple intensity comparisons in a small neighbourhood around the key point. However, ORB builds on top of these techniques by incorporating the issue of orientation invariance; it computes the orientation of each key point so that the algorithm can handle rotations and rotates the binary descriptors according to the computed key point orientation. When comparing the features from the image, the position change of the camera can be estimated.

Key features here include obstacles and hotspots predicted from the landmine detection environment. In a thermal image, these dots usually match the boundaries of a hotspot- where there is a clear temperature difference. Orientation Assignment: ORB computes an orientation depending on the intensity centroid for every detected keypoint, making the feature descriptor rotational resilient. Usually spanning 16 pixels, the FAST detector finds keypoints by comparing the intensity of a centre pixel I_c with that of surrounding pixels in a circular region. A pixel is said to be a keypoint if a continuous collection of N pixels is noticeably darker or brighter than I_c.

The FAST detector identifies keypoints by comparing the intensity of a centre pixel I_c with surrounding pixels in a circular region (usually 16 pixels). A pixel is considered a keypoint if a contiguous set of N pixels is significantly brighter or darker than I_c.

$$S(p) = \begin{cases} 1 & if\ I(p) > I_c + T\ or\ I(p) < I_c - T \\ 0 & otherwise \end{cases} \quad (1)$$

Where:

I(p) is the intensity of a surrounding pixel,
I_c is the centre pixel intensity,
T is a threshold,
S(p) determines whether a pixel is a keypoint.

3.1.3 Keypoint Orientation using Intensity Moments

ORB computes orientation using image moments to provide rotation invariance. The moments are calculated as:

$$m_{pq} = \sum_x \sum_y x^p y^q I(x, y) \quad (2)$$

The centroid of the patch around a keypoint is

$$C_x = \frac{m_{10}}{m_{00}}, C_y = \frac{m_{01}}{m_{00}} \quad (3)$$

The orientation angle is given by:

$$\theta = \tan^{-1}\left(\frac{m_{01}}{m_{10}}\right) \quad (4)$$

3.1.4. Feature Description and Rotated BRIEF

ORB generates a binary descriptor to represent each keypoint after its detection. Therefore, effective for matching and capturing the local intensity pattern. In thermal photos where the contrast could be slight, the binary descriptors remain powerful to noise and small illumination variations. ORB rotates the patch in line with the keypoint orientation θ, therefore modifying BRIEF (Binary Robust Independent Elementary Features). Computations of BRIEF descriptors are

$$d_i = \begin{cases} 1 & I(p_i) < I(q_i) \\ 0 & otherwise \end{cases} \quad (5)$$

Where: p_i, q_i are sampled pixel pairs in the patch, d_i is a binary descriptor bit.

Extending the area of view by combining several thermal images into a single, representative image requires image stitching, which also improves resolution. Density-Based Spatial Clustering of Applications with Noise (DBSCAN) provides a workable solution. It filters unnecessary keypoints while representing important image elements and excelling at spotting dense clusters of ORB keypoints. DBSCAN's capacity to dynamically ascertain the number of clusters depending on the density of keypoints, by not depending on predefined cluster count, is a major advantage over techniques as K_{means}. Extraction of the (x, y) pixel coordinates of all found ORB keypoints in both thermal images that match starts the clustering process. These coordinates then undergo the DBSCAN algorithm. Two main parameters define DBSCAN: minPts, which indicates the minimum number of keypoints needed to create a valid cluster, and epsilon (ε), which defines the radius of which surrounding keypoints are regarded as part of the same cluster. Keypoints outside of any cluster are seen as noise. Though these parameters should be finetuned depending on picture resolution, feature scale, and noise details of applications, they could be set to a number like 20 pixels and minPts to 5 in a normal implementation. Feature points are derived by applying DBSCAN to ORB keypoints. These clusters provide a more consistent picture of feature correlation. Utilizing ORB features in more reliable clusters, the resulting input to the RANSAC algorithm becomes significantly more robust, leading to improved accuracy and stability in camera position estimation. The average Euclidean distance between matched keypoints in image1 and image2 before applying any transformation is given by.

$$RMSE = \sqrt{\frac{1}{N}\sum_{i=1}^{N}(x_1 - x_2)^2 + (y_1 - y_2)^2} \quad (6)$$

where (x_1, y_1) and (x_2, y_2) are matched feature points.

3.2. ANN-Based Landmine Classification

An object's thermal signature is its temperature variation relative to its background. Because of variations across material composition along with thermal conductivity, buried landmines, which typically preserve a heat difference from their surroundings, tend to be especially helpful in identification. A low thermal signature implies that the object is either a part of the terrain or a non-threatening impediment; a high thermal signature suggests a buried landmine exists.

Stone, rock, and grass naturally occur in the robot environment. As it is difficult to distinguish the hot spot and obstacle in the thermal image due to imprecision and the ambiguous nature of the environment, a Multilayer Perceptron (MLP) is used in this work.

3.2.1. Based Classification

ANN using a Multilayer Perceptron (MLP) model was designed to detect and classify landmines by combining thermal image data and binary occupancy grid maps, as shown in Figure 2. Thermal images provided important features like heat intensity and temperature differences, and highlighted hot regions (called thermal signatures). At the same time, the binary occupancy grid showed which parts of the area were free and which had obstacles, using a simple black-and-white map. Before giving the data to the ANN, both the thermal and grid data were pre-processed: the thermal data was normalized to remove noise, and the 2D occupancy grid was converted into a 1D vector. These two data types were merged into a single input vector that captured heat and position information. The MLP model had an input layer based on the number of features, two hidden layers (with 256 and 128 neurons), and a softmax output layer that predicted whether a region contained an obstacle, a surface landmine, or a buried landmine.

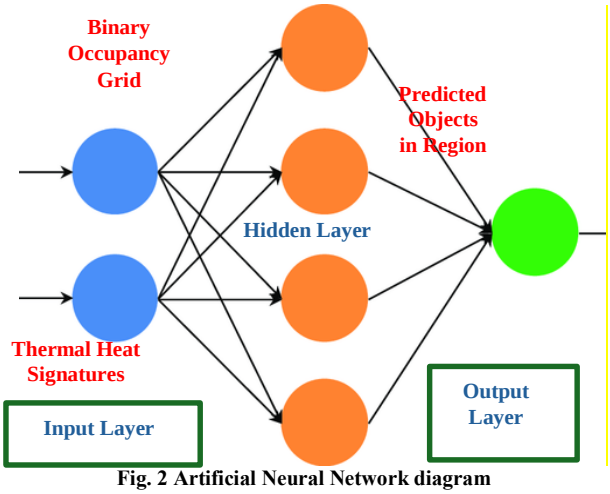

Fig. 2 Artificial Neural Network diagram

This combined approach helped the system make better decisions, especially in real-world environments where heat signals and terrain details can be complex or unclear.

Key classification metrics-precision, recall, and F1-score were calculated for each class using a confusion matrix. Precision is the percentage of accurately predicted samples among all predicted samples that belong to a specific class. Recall is the percentage of correctly predicted samples out of all actual samples that belong to that class. The F1 score provides a balanced measure by taking the harmonic mean of precision and recall, giving a single value that reflects both the accuracy and completeness of the classification. For each class, the True Positives (TP), False Positives (FP), and False Negatives (FN) were found; the resulting statistics are shown in Table 2.

3.3. Camera Calibration and Camera Position Estimation

Thermal camera calibration is carried out to convert image coordinates to world coordinates. Accurate temperature measurements, which are essential for differentiating landmines from the surrounding environment while accounting for emissivity, depend heavily on proper calibration. Inadequate calibration can lead to hazardous false positives or negatives. Using ORB feature extraction, features from consecutive images are then compared to estimate the current camera position, facilitating mobile robot localization. Intrinsic parameters define the internal characteristics of the camera, such as focal length and optical distortions. These parameters are independent of the camera's position or orientation in the environment. One of the key intrinsic parameters is the focal length (f_x, f_y), which determines how much the camera magnifies the objects. This varies for both the x and y axes and is measured in pixels. Another important attribute is the main point (c_x, c_y), which is the image sensor's center when the optical axis intersects with the image plan. It generally lies near the middle of the image, but it may shift due to lens aberrations. Skew coefficient – if the camera is distorted, this number outputs how much the x and y axes are rotated with respect to one another: this number should output 0 if the camera is perfect. Also, lens distortion coefficients consider the radial and tangential distortions that the lens itself causes. The intrinsic parameters are necessary for projecting 3D world coordinates to 2D image coordinates.

$$\begin{bmatrix} X_{camera} \\ Y_{camera} \\ Z_{camera} \end{bmatrix} = K^{-1}.E.\begin{bmatrix} X_{world} \\ Y_{world} \\ Z_{world} \\ 1 \end{bmatrix} \quad (7)$$

$$K = \begin{bmatrix} f_x & s & c_x \\ 0 & f_y & c_y \\ 0 & 0 & 1 \end{bmatrix} \quad (8)$$

$$f_x = \frac{W}{2\tan\left(\frac{\theta_x}{2}\right)} \quad (9)$$

$$f_y = \frac{H}{2\tan\left(\frac{\theta_y}{2}\right)} \quad (10)$$

The intrinsic matrix K converts 3D world coordinates into image pixel coordinates. Extrinsic parameters allow the conversion of real-world coordinates to the camera's coordinate system by defining its position and orientation with respect to the fixed world coordinate system. Understanding the camera's spatial orientation and position depends on these values. When determining why a camera is tilted or just rotated around various axes, the rotation matrix (R) shows the camera's orientation with regard to the world. Furthermore, the translation vector (T) specifies the camera's relative position to the world origin, therefore enabling the estimation of the camera's displacement about a reference point. These values taken together provide the extrinsic parameter matrix [E], stated as:

$$[E] = \begin{bmatrix} R & T \\ 0 & 1 \end{bmatrix} \quad (11)$$

This turns world coordinates to the reference frame of the camera. Applications, including 3D reconstruction, localization, and mapping, depend on this change since it allows the right projection from real-world points to the image plane.

3.4. Goal-Seeking RRT Algorithm

Based on the identified ORB features in the thermal image and the thermal image–based occupancy grid map, a multi–goal-seeking RRT algorithm is employed. The RRT-based path planning and obstacle avoidance algorithm is utilized to navigate an autonomous mobile robot towards the inspection of hotspots for mine detection while avoiding obstacles. This approach also describes the obstacle avoidance behaviour using RRT for safer robot navigation in mine areas, thereby enhancing detection precision and minimizing hazards for human operators.

3.4.1. Steps Involved in RRT Algorithm

Step 1: Node Expansion

Each node in the tree represents a state or position, and the RRT algorithm expands the tree by selecting a random point in the environment and connecting it to the nearest node in the existing tree. Let the current node be q_i, and a randomly sampled point be q_{rand}. The objective is to extend the tree from q_i toward q_{rand}.

Step 1: Find the nearest node

$$q_{nearest} = \arg\ min_{q_i} \|q_i - q_{rand}\| \quad (12)$$

where $\|q_i - q_{rand}\|$ It is the Euclidean distance between two points.

Step 2: Compute the direction toward the random point

$$q_{new} = q_{nearest} + \Delta t. \left(\frac{q_{rand} - q_{nearest}}{\|q_{rand} - q_{nearest}\|} \right) \quad (13)$$

Where Δt is the step size, and q_{new} is the new node added to the tree.

Step 3: Collision Check

The newly generated node q_{new} must be verified to ensure it remains free from collisions with obstacles in the environment. The new node q_{new} must be checked to ensure it does not collide with obstacles in the environment. If the path from $q_{nearest}$ to q_{new} intersects an obstacle, the node is rejected. This is typically checked using a line-of-sight test or a ray-casting algorithm.

Step 4: Adding the Node

Once the collision checks pass, the new node q_{new} is added to the tree as a child of $q_{nearest}$.

$$T = T \cup \{q_{new}\} \quad (14)$$

Where q_{goal} is the goal position, and ϵ is a small threshold value.

Step 5: Final Path Reconstruction

After reaching the goal, the path is reconstructed by tracing back from the goal node to the start node.

$$Path = \{q_0, q_1, \ldots, q_{goal}\} \quad (15)$$

3.5. Multi-Goal-Seeking Mobile Robot

In autonomous mobile robotics, goal-seeking behaviour is a crucial aspect of navigation. The mobile robot must move from a given starting coordinate to a goal position while maintaining stable motion and orientation. The orientation of the robot is determined using the straight-line equation connecting the start and goal points.

The RRT algorithm achieves numerous goals progressively through a staged procedure. RRT is employed to devise a trajectory from the initial position to Goal 1. Upon the discovery of this approach, Goal 1 becomes the role of the new beginning point. The RRT is subsequently re-initialized to produce a path from Goal 1 to Goal 2.

Each phase encompasses conventional RRT procedures: sampling, nearest node identification, steering, and collision assessment. The ultimate route is established by merging the paths from Start to Goal 1 and Goal 1 to Goal 2, ensuring the goals are attained in the specified sequence.

By means of simultaneous route planning to several landmines, the multi-goal seeking RRT algorithm increases the adaptability and efficiency of landmine detection robots. With ORB-based feature matching, thermal images are processed to extract the features, whereby calibrated feature points are transformed from pixel to world coordinates to map the hotspot location exactly with intrinsic and extrinsic matrices. The proposed multi-goal seeking method allows reaching the goal depending on ANN classification - buried, surface landmines, and obstacles.

Unlike running separate RRTs for each goal, it constructs a single tree with branches pointing to different objectives, hence greatly lowering computation time. When more than one goal is detected, Multi-goal RRT dynamically adjusts to environmental changes without restarting the planning process. The binary occupancy grid map from thermal image provides the details of the environment and effective navigation by providing free space and obstacle data to execute the multi-goal RRT.

The robot can detect the landmines efficiently by combining ANN classification, ORB-based localisation, and a multi-goal RRT algorithm with real-time cost metrics like time taken to reach the goal and path length to get optimized results.

3.5.1. Flowchart of Multi-Goal Seeking RRT

The proposed Multi-Goal Seeking RRT algorithm is designed to efficiently generate feasible paths to multiple targets within a cluttered environment. As illustrated in Figure 3, the algorithm is initialized by defining the environment, including the start node and the spatial locations of two goal nodes (Goal 1 and Goal 2).

Both goals are initially marked as unreached, and the exploration process is driven by a main iterative loop that continues until either both goals are successfully attained or a predefined maximum number of iterations is reached.

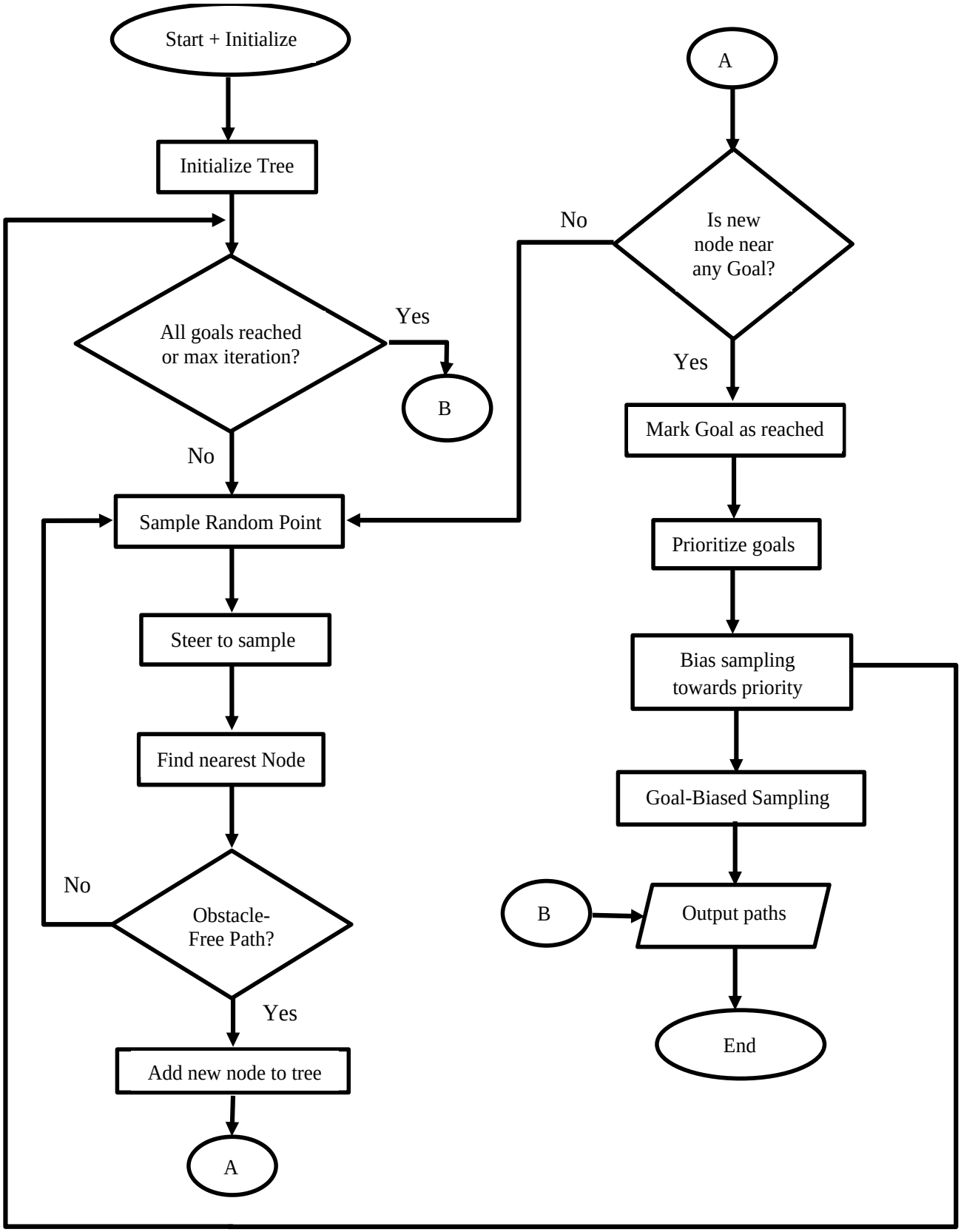

Fig. 3 Flowchart of the multi-goal seeking algorithm

The algorithm samples a random position within the search space at each iteration. To improve convergence efficiency, the sampling technique incorporates a bias toward the nearest unreached goal, thereby directing the expansion of the tree closer to the desired targets. Following the sampling stage, the nearest node in the existing tree is identified, and a steering step generates a new node by incrementally extending the tree toward the sampled point. A collision-checking routine is executed to ensure that the newly created edge connecting the nearest node to the new node is free from obstacles before appending the node to the structure.

Once incorporated, the algorithm evaluates whether the new node lies within a specified threshold distance of Goal 1 or Goal 2. If the condition is satisfied, the corresponding goal is marked as reached. Through recursive expansion, the tree progressively establishes connections from the start node to the goal nodes while simultaneously exploring the environment and avoiding obstacles.

The process stops when both goal nodes have been reached or when the termination criterion is met. At completion, the resulting tree structure provides valid, collision-free paths from the start node to each goal, demonstrating the effectiveness of the proposed Multi-Goal Seeking RRT in multi-target navigation scenarios.

4. Results and Discussion

4.1. Binary Occupancy Grid Map Generation and ANN-based Hotspot Classification

The binary occupancy grid map produced from RGB and Thermal images was separately shown in Figures 5(a) and (b), respectively. The figure shows that the occupancy grid from the thermal image offers a more exact depiction of the environmental hotspot. It records the temperature changes to explain improved accuracy by facilitating the classification of various environmental features. The thermal-based occupancy grid guarantees consistent and precise mapping of surroundings, unlike RGB images, which are affected by lighting conditions as well as shadows. An experimental configuration of 3 × 4 meters was constructed to replicate real minefield circumstances to evaluate the proposed landmine detection system, as shown in Figure 4. The landscape was created to include both surface and buried landmines placed at various depths that replicate real-world unpredictability. In addition, artificial impediments such as rocks, irregular terrain, and grass were positioned across the area to mimic the intricate, congested environment that is commonly faced in real demining operations.

These barriers presented physical hurdles for navigation and functioned as non-mine heat signatures in thermal images, complicating detection and classification operations. The configuration facilitated an extensive assessment of the autonomous robot's sensory, classification, and path-planning abilities in near-realistic situations. Thermal imaging sensors, together with an ANN classifier, were utilised for hotspot identification, whereas the robot implemented ORB-based feature matching and a multi-goal-seeking RRT algorithm for localisation and navigation. The complete configuration was designed to offer a regulated yet demanding testing environment that connects simulation with field implementation.

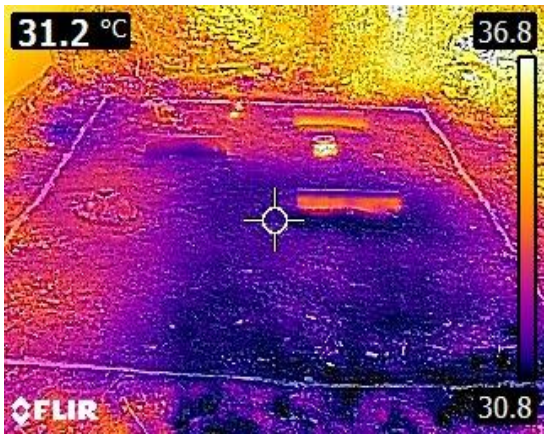

Fig. 4 Thermal image of cluttered experimental test environment

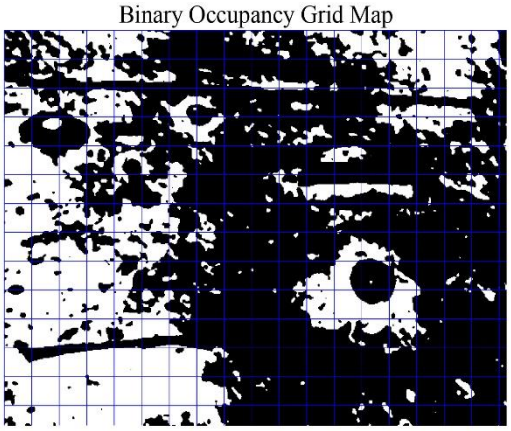

Fig. 5(a) Grid map representation of an RGB image

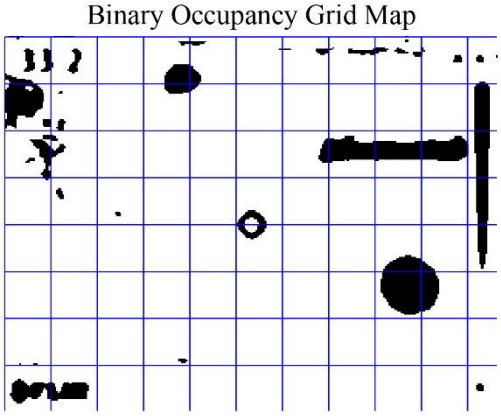

Fig. 5(b) Grid map representation of thermal image

Figure 6 shows the classified results from the ANN hotspot, obstacle from the ultrasonic sensor time delay distance, and thermal signature from the thermal camera. Employing a grid map within ANN classification allows precise obstacle localization by correlating thermal intensities to discrete cells. Using ANN rules allows dynamic object classification and separation of hotspots, obstacles, and safe zones. This organized technique improves safe path planning for landmine detection robots to avoid obstacles and navigate effectively. Moreover, it enhances real-time environment perception through the fusion of multi-sensor data for adaptive locomotion. The performance of the ANN classifier was evaluated using a confusion matrix derived from the testing phase. The confusion matrix, as shown in Figure 7, illustrates the relationship between the actual and predicted class labels across three classes: Obstacle, Surface Landmine, and Buried Landmine. Key classification metrics such as Precision, Recall, and F1-score may be derived from the confusion matrix and are listed in Table 1. The diagonal numbers show great class-specific recognition capacity. Off-diagonal values show particular confusion patterns that direct feature extraction and model refinement changes. Examining training and testing confusion matrices side by side helps to identify underfitting or overfitting behaviour. Detection of systemic biases or weaknesses in classification might guide techniques like architecture tuning or dataset augmentation.

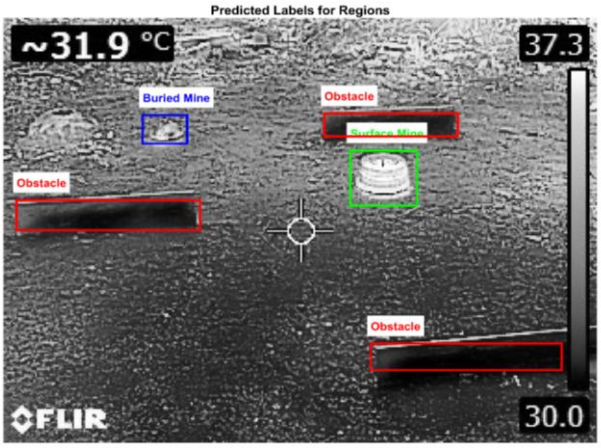

Fig. 6 Classification of hotspot, obstacle

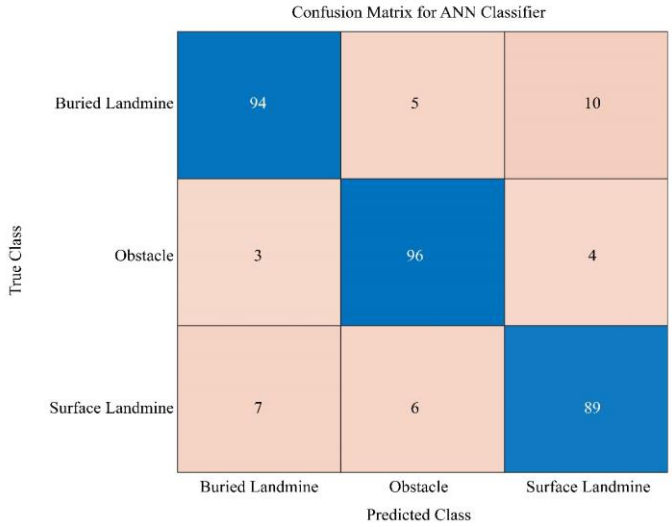

Fig. 7 Confusion matrix

Table 1. Performance evaluation metrics

Class	TP	FP	FN	Pre-cision (%)	Recall (%)	F1 score (%)
Class 1 (obstacle)	89	11	7	89.00	92.71	90.82
Class 2 (Surface Landmine)	92	14	13	86.79	87.62	87.20
Class 3 (Buried Landmine)	94	10	15	90.38	86.24	88.26

A confusion matrix has been created to determine the efficiency of the ANN-based landmine classification system, and essential metrics such as Precision, Recall, and F1-Score were calculated for each category: Obstacle, Surface Landmine, and Buried Landmine. Class 1 (Obstacle) obtained a Precision of 89.00%, signifying that the majority of obstacle predictions were accurate, and a Recall of 92.71%, demonstrating the model's robust capability to accurately identify obstacles. The F1-Score, a harmonic mean of Precision and Recall, was 90.82%, indicating balanced performance. Class 2 (Surface Landmine) demonstrated a Precision of 86.79% and a Recall of 87.62%, yielding an F1-score of 87.20%, indicating dependable detection of surface landmines with few false positives. Class 3 (Buried Landmine) attained a Precision of 90.38% and a Recall of 86.24%, resulting in an F1-Score of 88.26%. This indicates that buried landmines were categorised with a robust equilibrium between sensitivity and specificity.

4.2. Camera Calibration

This work calibrated the FLIR E6390 thermal camera with a focal length of 0.6mm against a known dimension rectangular box (33.5cm * 22.5 cm). Image coordinates are transformed to world coordinates through a calibration pattern observable to both infrared and RGB cameras.

The resultant intrinsic camera matrix k is $K = \begin{bmatrix} 0.16 & 0 & 160 \\ 0 & 0.16 & 120 \\ 0 & 0 & 1 \end{bmatrix}$

This matrix allows the translation of image pixels to world coordinates, as evident from the sample mappings, and is given in Table 2, where u and v are camera coordinates and X and Y are world coordinates. These mappings play a very significant role in usage, such as rendering 3D thermal image processing.

Table 2. Mapped test pixels to world coordinates

Pixel_X (u)	Pixel_Y(v)	World_X(X)	World_Y(Y)
176	216	7.3357	56.996
100	100	62.636	1.5007
150	101	61.873	38.197
283	216	6.8322	132.5

The extrinsic matrix E helps in estimating the camera's actual position in the environment. The values (54.67, 34.78) represent the estimated translation of the camera in the x and y directions within the image plane. This information is typically used in image stitching and position tracking, where the camera's movement between two frames is analysed. The coordinates (160,120, -0.6) describe the camera's estimated position in 3D space relative to a reference frame. The X and Y values correspond to positions parallel to the image plane, while Z represents the distance from the camera to the reference plane. The camera is slightly behind the reference plane, indicating a minor backward shift. The rotation vector represents the camera's orientation in 3D space. These values correspond $\begin{bmatrix} -0.0330 \\ 0.0230 \\ 0.4769 \end{bmatrix}$ To rotations around the X, Y, and Z axes. The vector can be converted into a rotation matrix for further interpretation, which helps to understand how the camera has rotated relative to the reference frame. The rotation vector represents the camera's orientation in 3D space. These values correspond to rotations around the X, Y, and Z axes. The vector can be converted into Euler angles or a rotation matrix for further interpretation, which helps understand how the camera has tilted or rotated relative to the reference frame. Figure 8 presents the original thermal image captured using the FLIR E6390 thermal camera.

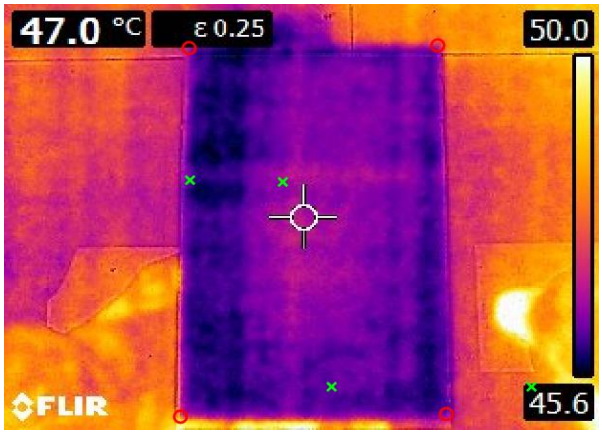

Fig. 8 Thermal camera calibration

4.3. ORB-Based Feature Matching and Camera Pose Estimation

Feature matching across consecutive frames enables the estimation of camera pose within image sequences. ORB features are first extracted from both input images and then matched. Homography and the RANSAC (Random Sample Consensus) algorithm are applied to ensure robustness and eliminate outliers. The resulting orientation data are recorded in tabular form, providing the x- and y-axis orientations derived from matched features. Camera pose is subsequently estimated using the Perspective-n-Point (PnP) function, which provides accurate localization of the relative camera position. In addition, input images are stitched using standard image stitching methods to generate an enhanced representation of the surrounding environment. Such representations are particularly intuitive for robotic navigation and augmented reality applications, where spatial awareness is critical. Figure 9(a) and 9(b) show the thermal input images used for ORB feature matching, while Figure 9(c) illustrates the detected ORB correspondences before RANSAC. The image for enhanced environmental visualization after RANSAC is shown in Figure 9(d). Feature correspondences between the thermal images and 2 corresponding X and Y coordinate data

are provided in Table 3. Root Mean Square Error (RMSE) values are reported before and after alignment as 65.7483 pixels and 63.1836 pixels, respectively. The reduction in RMSE indicates improved alignment accuracy, thereby validating the efficiency of ORB-based matching. RMSE serves as a key metric for evaluating image registration accuracy, where lower values correspond to more precise feature matching. DBSCAN clustering is applied to the ORB keypoints to refine correlation further, producing more consistent feature groupings in the thermal imagery.

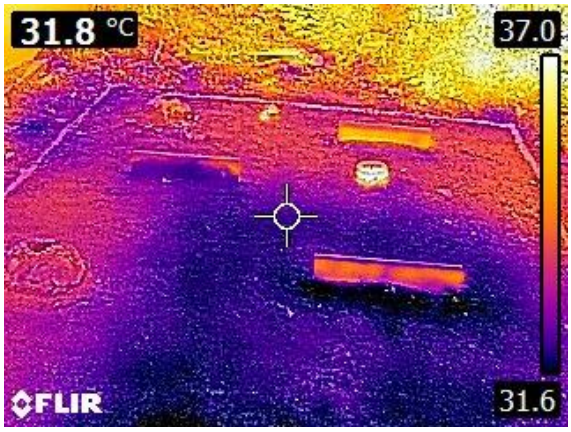

(a) Image 1

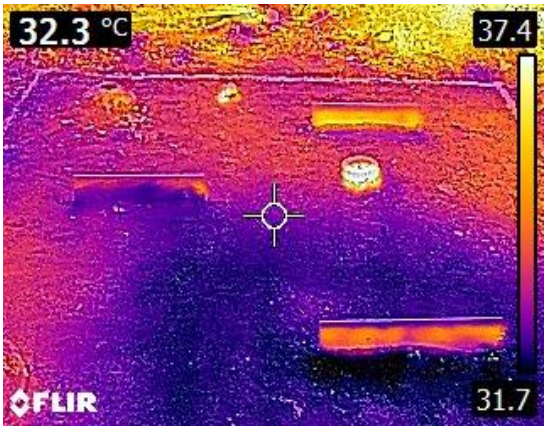

(b) Image 2

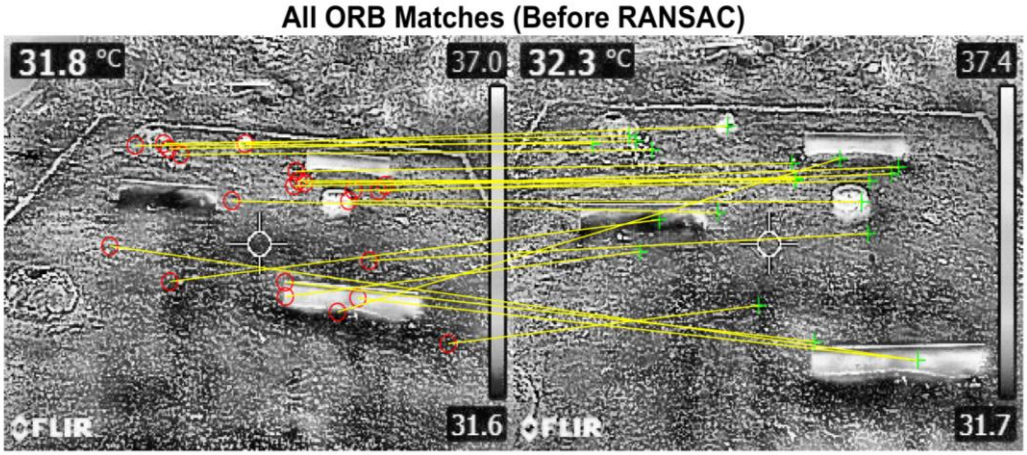

(c) ORB feature mapping

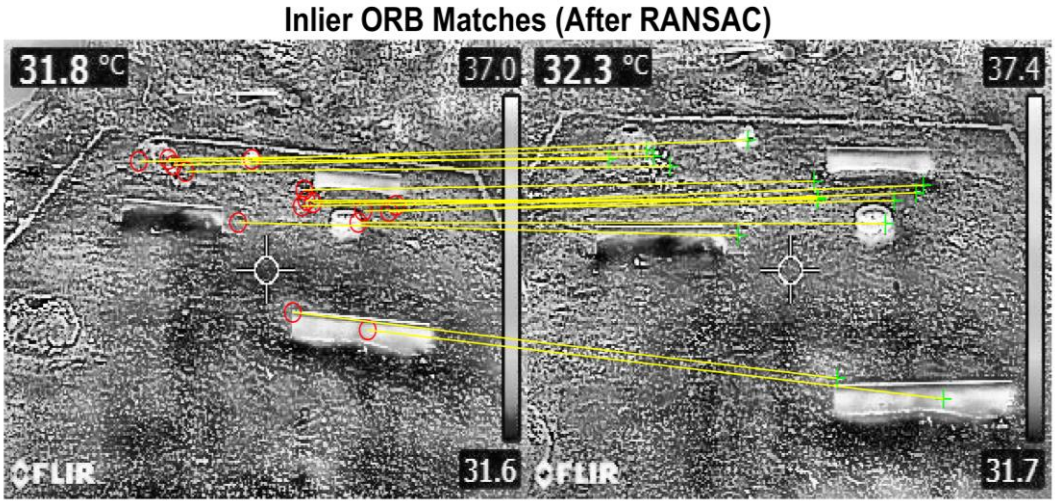

(d) Feature mapping from image 1 to image 2

Fig. 9 ORB-based Feature extraction from Thermal image

Table 3. Feature matching from thermal image 1 to thermal image 2

Sl. No	Image1_ X	Image1_ Y	Image2_ X	Image2_ Y	Delta_ X	Delta_ Y	Theta (rad)	Theta(degrees)
1.	157	34	41.8	124.6	-115.2	90.6	2.4752	141.82
2.	208	35	288	168	80	133	1.0293	58.97
3.	210	35	288	168	78	133	1.0404	59.61
4.	75	39	209	117	134	78	0.52715	30.2
5.	101	49	249.83	102.95	148.83	53.95	0.34777	19.93
6.	247	58	241.48	179.56	-5.52	121.56	1.6162	92.6
7.	98	61	264	194	166	133	0.67548	38.7
8.	193	77	253	71.8	60	-5.2	-0.08645	355.05
9.	128	79	165	88	37	9	0.23861	13.67
10.	251	79	226	108	-25	29	2.2823	130.76
11.	164	92	204.21	168.96	40.21	76.96	1.0893	62.41
12.	139	93	191	94	52	1	0.019228	1.1
13.	124	94	222	40	98	-54	-0.50363	331.14
14.	111	97	243.61	171.04	132.61	74.04	0.50918	29.17
15.	134	98	189	100	55	2	0.036348	2.08
16.	154	104	238	195	84	91	0.82538	47.29
17.	116	111	120.23	180.71	4.23	69.71	1.5102	86.53
18.	287	113	220.46	59.75	-66.54	-53.25	-2.4667	218.67
19.	111	117	161.8	123.4	50.8	6.4	0.12532	7.18
20.	114	118	171.4	125.8	57.4	7.8	0.13506	7.74
21.	195	118	251	118	56	0	0	0
22.	112	120	169	127	57	7	0.1222	7
23.	71	131	123	105	52	-26	-0.46365	333.43
24.	153	135	273.4	101.8	120.4	-33.2	-0.26906	344.58
25.	59	160	128.87	182.44	69.87	22.44	0.31075	17.8

4.4. Multi-Goal Seeking RRT

The Multi-Goal Seeking RRT algorithm was evaluated in a mine detection environment by integrating ANN-based prediction with ORB feature extraction for target localization.

The experimental setup involved navigation from starting coordinates (2.0, 0.5) to two distinct targets: Goal 1 (surface landmine at 2.0, 2.5) and Goal 2 (buried landmine at 1.2, 3.5). Target coordinates were determined through ORB feature matching to enhance localization accuracy while accounting for environmental obstacles.

Table 4 presents a comprehensive performance comparison between the proposed Multi-Goal Seeking RRT and conventional path planning algorithms (RRT, RRT*, and goal-seeking RRT). The results demonstrate significant improvements across multiple performance metrics.

Computational Efficiency: The proposed algorithm achieved both goals in 1.2 seconds, substantially outperforming conventional approaches that require sequential goal visits with return-to-start iterations, resulting in increased computation time.

Path Planning Metrics: The algorithm required only 210 iterations to reach both targets while visiting 108 nodes during tree expansion. This represents a 67% reduction compared to conventional RRT (333 nodes) and a 77% reduction compared to RRT* (465 nodes), indicating superior sampling efficiency and goal-directed exploration.

Path Optimality: The generated path length of approximately 4.0 meters to reach both goals demonstrates improved efficiency compared to single-goal approaches: conventional RRT (4.913 m) and goal-seeking RRT (4.233 m). This 19-23% improvement in path length directly translates to reduced energy consumption and mission time.

The superior performance of the Multi-Goal Seeking RRT results from its ability to simultaneously explore toward multiple objectives within a single search tree.

The integration with ORB-based feature matching enhances target localization precision, while the goal-biased sampling strategy accelerates convergence toward both landmine locations.

These results confirm that the proposed approach provides an efficient solution for multi-target navigation in mine detection scenarios, effectively balancing exploration overhead, planning time, and path optimality. Figure 10 summarizes the comparative performance analysis.

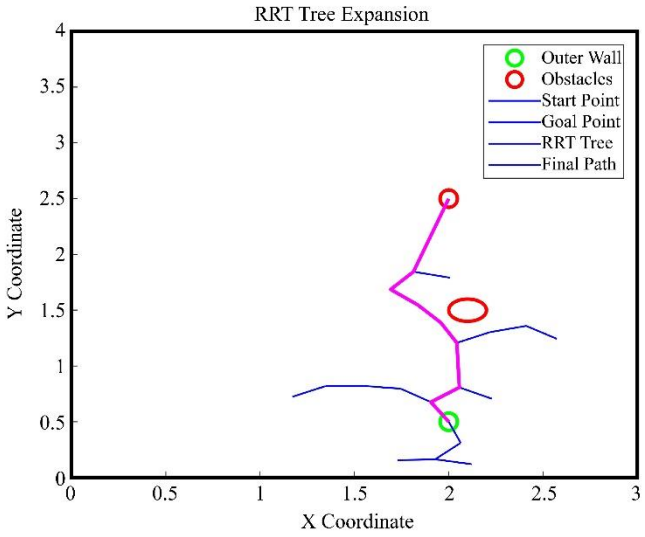

(a) RRT with a single obstacle

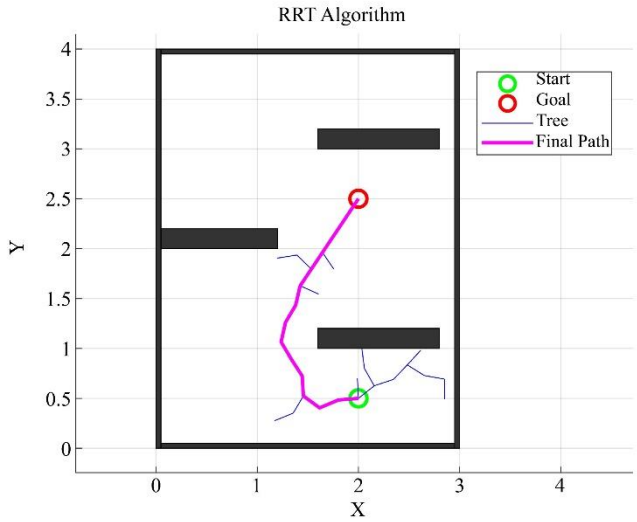

(b) RRT with multiple obstacles

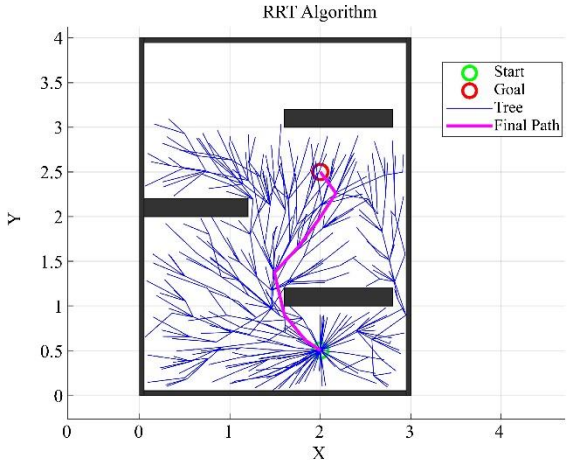

(c) RRT-star with multiple obstacles

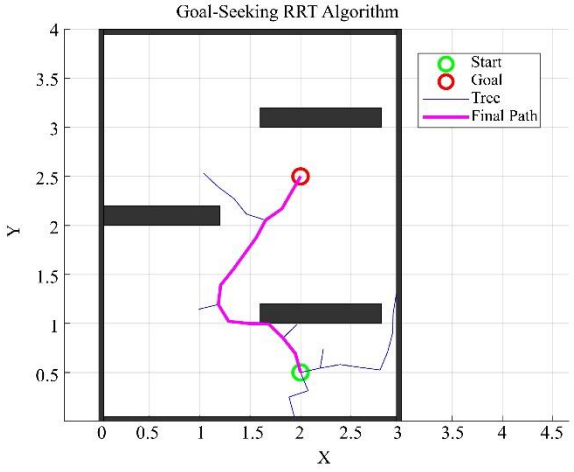

(d) Goal-seeking RRT with goal 1

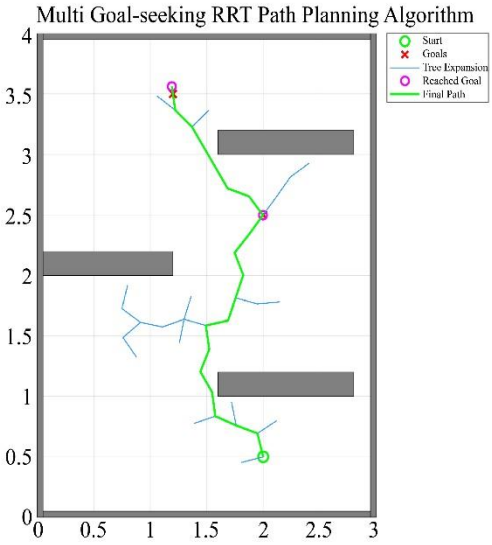

(e) Multi-goal seeking RRT

Fig. 10 Comparison of RRT-based Path Planning Algorithms

Table 4. Performance comparison of the proposed RRT algorithm

Algorithm	RRT	RRT *	Goal-seeking RRT	Multi-Goal Seeking RRT
	Goal 1	Goal 1	Goal 1	Both Goal 1 and Goal 2
Time taken (sec)	0.784	0.635	0.494	1.2
Iteration to reach the goal	270	256	180	210
Number of nodes visited	333	465	113	108
Path length (m)	4.913	4.138	4.233	4

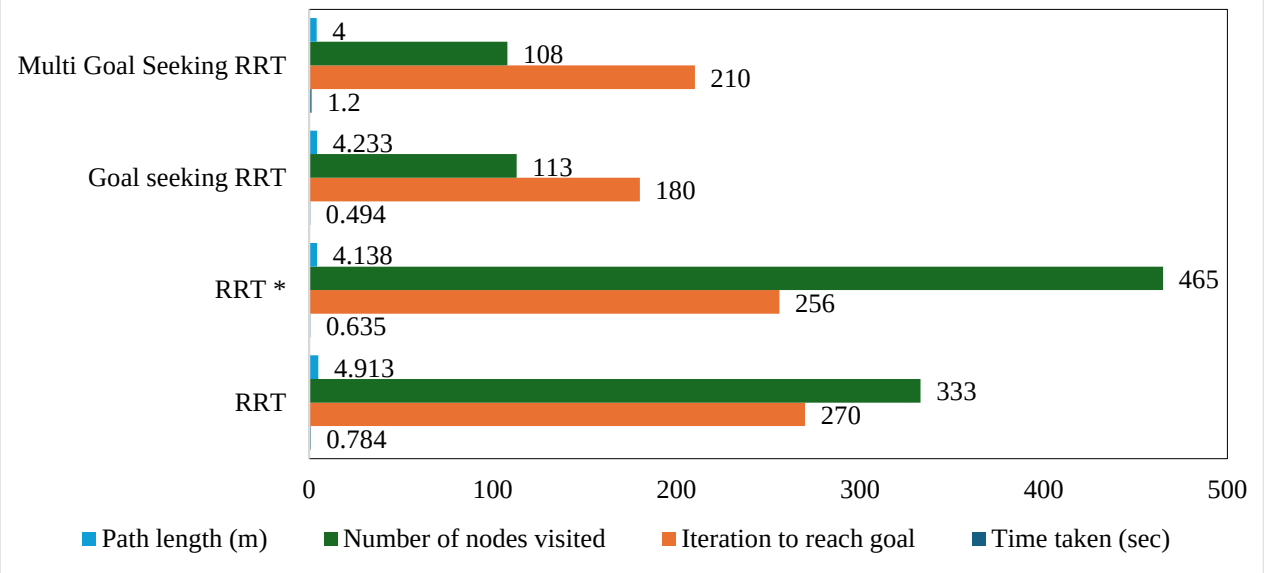

Fig. 11 Performance comparison of the proposed RRT algorithm

5. Conclusion

The proposed system integrates a binary occupancy grid map, ANN-based classification of landmine type and obstacles, ORB feature matching for camera pose estimation, and RRT-based obstacle avoidance that significantly enhances the performance of autonomous mobile robots in mine detection and exploration missions. From the binary occupancy grid map, the basic information from the thermal image can be easily understood for further classification. With the help of a binary occupancy grid map and thermal signature, the MLP classifies the hotspot.

This classification provides a more reliable method for identifying potential threats to improve the overall safety of the mission. The thermal camera calibration is carried out to get a precise location and convert the pixel coordinates to world coordinates from the thermal image. Using ORB feature matching and extraction from thermal images, the camera position and orientation can be estimated, enabling the robot to localize in GPS-denied environments.

The feature extraction and matching approach is found to provide a lower RMSE value before and after alignment, and it is found to be 65.7483 pixels and 63.1836 pixels, which highlights that the localization using ORB is efficient. The proposed feature extraction technique is more effective in real-time applications and complex terrain environments. A multi-goal seeking RRT-based path planning algorithm was employed to navigate efficiently in a cluttered environment, enabling the robot to dynamically plan safe, collision-free paths. The system achieved a path planning time of just 1.2 seconds.

Classification performance for surface and buried landmines showed high precision, recall, and F1-scores, confirming the system's accuracy. As a result, the system improves detection accuracy, minimizes operational risks, and ensures the safety of human operators, making it a promising solution for real-world mine detection applications.

Acknowledgments

The authors thank the European Commission for supporting this research project under the scheme ERASMUS-JMO-2023- HEI. Titled "Promoting European Union approach on Trustworthy Artificial Intelligence and Innovative Product Development Techniques for Digital Green Transformation" EU-TRIPOD, Proposal ID: 101127804.

Funding

This work received financial support from the Science and Engineering Research Board, New Delhi, under the "Teaching Associateship for Research Excellence" scheme (TAR/2018/001123).

References

[1] H. Kasban et al., "A Comparative Study of Landmine Detection Techniques," *Sensing and Imaging: An International Journal*, vol. 11, no. 3, pp. 89-112, 2010. [CrossRef] [Google Scholar] [Publisher Link]

[2] Johana Florez-Lozano et al., "Cooperative and Distributed Decision-Making in a Multi-Agent Perception System for Improvised Land Mines Detection," *Information Fusion*, vol. 64, pp. 32-49, 2020. [CrossRef] [Google Scholar] [Publisher Link]

[3] Prabin Kumar Panigrahi, and Sukant Kishoro Bisoy, "Localization Strategies for Autonomous Mobile Robots: A Review," *Journal of King Saud University - Computer and Information Sciences*, vol. 34, no. 8, pp. 6019-6039, 2022. [CrossRef] [Google Scholar] [Publisher Link]

[4] Francisco Rubio, Francisco Valero, and Carlos Llopis-Albert, "A Review of Mobile Robots: Concepts, Methods, Theoretical Framework, and Applications," *International Journal of Advanced Robotic Systems*, vol. 16, no. 2, pp. 1-22, 2019. [CrossRef] [Google Scholar] [Publisher Link]

[5] A. Bhuiyan, and B. Nath, "Anti-Personnel Mine Detection and Classification Using GPR Image," *18th International Conference on Pattern Recognition (ICPR'06)*, Hong Kong, China, vol. 2, pp. 1082-1085, 2006. [CrossRef] [Google Scholar] [Publisher Link]

[6] T. Fukuda et al., "Environment-adaptive Anti-personnel Mine Detection System: Advanced Mine Sweeper," *Using Robots in Hazardous Environments*, pp. 285-298, 2011. [CrossRef] [Google Scholar] [Publisher Link]

[7] Serkan Kaya, and Ugur Murat Leloglu, "Buried and Surface Mine Detection from Thermal Image Time Series," *IEEE Journal of Selected Topics in Applied Earth Observations and Remote Sensing,* vol. 10, no. 10, pp. 4544-4552, 2017. [CrossRef] [Google Scholar] [Publisher Link]

[8] A.O. Ajlouni, and A.F. Sheta, "A Novel Landmine Detection Process Using Karhunen Loeve Transform and Marker-Based Watershed Segmentation in IR Images," *International Journal of Signal and Imaging Systems Engineering (IJSISE)*, vol. 3, no. 1, pp. 21-30, 2010. [CrossRef] [Google Scholar] [Publisher Link]

[9] Bhavesh Deshpande et al., "Matching as Color Images: Thermal Image Local Feature Detection and Description," *ICASSP 2021 - 2021 IEEE International Conference on Acoustics, Speech and Signal Processing (ICASSP)*, Toronto, ON, Canada, pp. 1905-1909, 2021. [CrossRef] [Google Scholar] [Publisher Link]

[10] Lixing Liu et al., "Path Planning Techniques for Mobile Robots: Review and Prospect," *Expert Systems with Applications*, vol. 227, pp. 1-30, 2023. [CrossRef] [Google Scholar] [Publisher Link]

[11] Di Feng et al., "Deep Multi-Modal Object Detection and Semantic Segmentation for Autonomous Driving: Datasets, Methods, and Challenges," *IEEE Transactions on Intelligent Transportation Systems*, vol. 22, no. 3, pp. 1341-1360, 2021. [CrossRef] [Google Scholar] [Publisher Link]

[12] Ivan T. Ćirić et al., "Thermal Vision Based Intelligent System for Human Detection and Tracking in Mobile Robot Control System," *Thermal Science*, vol. 20, no. 5, pp. S1553-S1559, 2016. [CrossRef] [Google Scholar] [Publisher Link]

[13] A. Vinay et al., "ORB-PCA Based Feature Extraction Technique for Face Recognition," *Procedia Computer Science*, vol. 58, pp. 614-621, 2015. [CrossRef] [Google Scholar] [Publisher Link]

[14] Yunpeng Sun, and Xiaoli Li, "Feature Extraction and Matching Combined with Depth Information in Visual Simultaneous Localization and Mapping," *International Journal of Advanced Robotic Systems,* vol. 20, no. 2, pp. 1-15, 2023. [CrossRef] [Google Scholar] [Publisher Link]

[15] Surbhi Gupta, Munish Kumar, and Anupam Garg, "Improved Object Recognition Results Using SIFT and ORB Feature Detector," *Multimedia Tools and Applications*, vol. 78, no. 23, pp. 34157-34171, 2019. [CrossRef] [Google Scholar] [Publisher Link]

[16] Chuan Liao, Yinghua Liao, and Jun Xie, "Obstacle Avoidance Trajectory Planning of Loading Robot Based on Improved RRT Algorithm," *International Core Journal of Engineering*, vol. 5 no. 6, pp. 209-213, 2020. [CrossRef] [Google Scholar] [Publisher Link]

[17] Iram Noreen, Amna Khan, and Zulfiqar Habib, "Optimal Path Planning using RRT* based Approaches: A Survey and Future Directions," *International Journal of Advanced Computer Science and Applications*, vol. 7, no. 11, pp. 97-107, 2016. [CrossRef] [Google Scholar] [Publisher Link]

[18] Jiankun Wang, Max Q.H. Meng, and Oussama Khatib, "EB-RRT: Optimal Motion Planning for Mobile Robots," *IEEE Transactions on Automation Science and Engineering*, vol. 17, no. 4, pp. 2063-2073, 2020. [CrossRef] [Google Scholar] [Publisher Link]

[19] Gabrielle Hedrick, Nicholas Ohi, and Yu Gu, "Terrain-Aware Path Planning and Map Update for Mars Sample Return Mission," *IEEE Robotics and Automation Letters*, vol. 5, no. 4, pp. 5181-5188, 2020. [CrossRef] [Google Scholar] [Publisher Link]

[20] Ikram Ullah, and Kai Siong Yow, "Automated Vehicle Dent Detection Using Hybrid Image Processing and Fuzzy Decision Making," *Mechatronics and Intelligent Transportation Systems*, vol. 4, no. 1, pp. 49-60, 2025. [CrossRef] [Google Scholar] [Publisher Link]

[21] M. Oprea, "Agent-based Modelling of Multi-Robot Systems," *IOP Conference Series: Materials Science and Engineering*, vol. 444, no. 5, pp. 1-8, 2018. [CrossRef] [Google Scholar] [Publisher Link]

[22] Bo Zhang et al., "Path Planning for Wheeled Mobile Robot in Partially Known Uneven Terrain," *Sensors*, vol. 22, no. 14, pp. 1-16, 2022. [CrossRef] [Google Scholar] [Publisher Link]

[23] Sebastian Gelfert, "A Sensor Review for Human Detection with Robotic Systems in Regular and Smoky Environments," *International Journal of Advanced Robotic Systems*, vol. 20, no. 3, pp. 1-11, 2023. [CrossRef] [Google Scholar] [Publisher Link]

[24] Safa Jameel Al-Kamil, and Róbert Szabolcsi, "Optimizing Path Planning in Mobile Robot Systems Using Motion Capture Technology," *Results in Engineering*, vol. 22, pp. 1 -9, 2024. [CrossRef] [Google Scholar] [Publisher Link]

[25] Husam A. Neamah, Elek Donát, and Péter Korondi, "Optimizing Autonomous Navigation in Unknown Environments: A Novel Trap Avoiding Vector Field Histogram Algorithm VFH+T," *Results in Engineering*, vol. 23, pp. 1-17, 2024. [CrossRef] [Google Scholar] [Publisher Link]

[26] Motoyuki Sato et al., "Landmine Detection by 3D GPR System," *Detection and Sensing of Mines, Explosive Objects, and Obscured Targets XVII*, SPIE, Baltimore, Maryland, United States, vol. 8357, pp. 322-330, 2012. [CrossRef] [Google Scholar] [Publisher Link]